MODELING OF PERFLUOROCARBONS DECOMPOSITION IN NITROGEN THERMAL PLASMA

S.W. CHAU^{a,*}, S.H. CHEN^b

^{a} *Department of Engineering Science and Ocean Engineering, National Taiwan University, 1, Sec. 4, Roosevelt Rd., 10617 Taipei, Taiwan, ROC*

^{b} *Physics Division, Institute of Nuclear Energy Research, 1000 Wenhua Rd., Longtan, 32546 Taoyuan, Taiwan, ROC*

* chausw@ntu.edu.tw

Abstract. This paper develops an axisymmetric flow model to predict the flow field inside a direct-current plasma torch reactor, where the magneto-hydrodynamic equations, including the continuity, momentum, energy and current continuity equations as well as turbulence transport equations are solved with a finite volume discretization in a segregated manner. The thermodynamic and transport coefficients of thermal plasma are obtained from the condition of local thermal equilibrium, whereas a kinetics model is employed to consider the production and destruction of species due to the chemical reactions in a decomposition process. Species transport phenomena arising in the decomposition process are described by the transport equations for different species. The perfluorocarbons decomposition characteristics in a well-type, non-transferred nitrogen torch reactor are analyzed by the proposed numerical model to disclose the influence of working parameters on the decomposition efficiency.

Keywords: perfluorocarbons decomposition, nitrogen, thermal plasma, direct-current, plasma torch.

1. Introduction

Compared with other methods to remove hazardous gases arising in modern industrial processing, thermal plasma delivers an advantage of removal efficiency, processing flexibility, operation safety and installation cost that attract the attention of recent researchers [1, 2]. Perfluorocarbon (PFC), such as CF_4, C_2F_6, and NF_3, can be first reduced into an atomic or molecular form of its chemical components in the high-temperature environment created by thermal plasma flow. A further introduction of water into the reacting process can enhance the production of HF and CO_2, which can be easily treated in the following processes. This paper is first to develops an axisymmetric flow model to predict the thermal plasma inside a direct-current torch reactor operating with nitrogen. The perfluorocarbons decomposition characteristics in a well-type, non-transferred plasma torch reactor are then analyzed by the proposed numerical model to disclose the influence of working parameters on the decomposition efficiency.

2. Thermal plasma model

The following assumptions are adopted for a steady and axisymmetric thermal plasma flow: The plasma is optically thin, the plasma is assumed in local thermal equilibrium, the gravitational effect and the external magnetic field is ignored. The magneto-hydrodynamic equations consisting of the continuity equation, momentum equation, energy equation, and current continuity equation are given as follows:
.

Continuity equation

$$\frac{\partial(\rho u)}{\partial z} + \frac{1}{r}\frac{\partial(\rho r v)}{\partial r} = 0 \qquad (1)$$

Momentum equation (axial-direction)

$$\frac{\partial(\rho u^2)}{\partial z} + \frac{1}{r}\frac{\partial(\rho r u v)}{\partial r} = -\frac{\partial p}{\partial z} + 2\frac{\partial}{\partial z}[\mu(\frac{\partial u}{\partial z})]$$
$$+ \frac{1}{r}\frac{\partial}{\partial r}[r\mu(\frac{\partial u}{\partial r} + \frac{\partial v}{\partial z})] + j_r B_\theta \qquad (2)$$

Momentum equation (radial-direction)

$$\frac{\partial(\rho u v)}{\partial z} + \frac{1}{r}\frac{\partial(\rho r v^2)}{\partial r} = -\frac{\partial p}{\partial y} + \frac{2}{r}\frac{\partial}{\partial r}[\mu r(\frac{\partial v}{\partial r})]$$
$$+ \frac{\partial}{\partial z}[\mu(\frac{\partial u}{\partial r} + \frac{\partial v}{\partial z})] - \mu(\frac{2v}{r^2}) + \frac{\rho w^2}{r} - j_z B_\theta \qquad (3)$$

Momentum equation (azimuthal-direction)

$$\frac{\partial(\rho u w)}{\partial z} + \frac{1}{r}\frac{\partial(\rho r v w)}{\partial r} = \frac{\partial}{\partial z}[\mu(\frac{\partial w}{\partial z})]$$
$$+ \frac{1}{r^2}\frac{\partial}{\partial r}[\mu r^3 \frac{\partial}{\partial r}(\frac{w}{r})] - \frac{\rho v w}{r} \qquad (4)$$

Energy equation

$$\frac{\partial(\rho u h)}{\partial z} + \frac{1}{r}\frac{\partial(\rho r v h)}{\partial r} = u\frac{\partial p}{\partial z} + v\frac{\partial p}{\partial r}$$
$$+ \frac{\partial}{\partial z}(k\frac{\partial T}{\partial z}) + \frac{1}{r}\frac{\partial}{\partial r}(rk\frac{\partial T}{\partial r}) + \frac{j_z^2 + j_r^2}{\sigma}$$
$$- S_R + \frac{5}{2}\frac{k_B}{e}(j_z\frac{\partial T}{\partial z} + j_r\frac{\partial T}{\partial r}) + \mu|\dot{\gamma}|^2 \qquad (5)$$

Turbulence model

$$\frac{\partial(\rho u K)}{\partial z} + \frac{1}{r}\frac{\partial(\rho v K)}{\partial r} = G - \rho\epsilon +$$
$$\frac{\partial}{\partial z}[(\mu_m + \frac{\mu_t}{\sigma_K})\frac{\partial K}{\partial z}] + \frac{1}{r}\frac{\partial}{\partial r}[(\mu_m + \frac{\mu_t}{\sigma_K})\frac{\partial K}{\partial r}] \quad (6)$$

$$\frac{\partial(\rho u \epsilon)}{\partial z} + \frac{1}{r}\frac{\partial(\rho v \epsilon)}{\partial r} = c_{\epsilon 1} G \frac{\epsilon}{K} - c_{\epsilon 2}\rho\frac{\epsilon^2}{K} +$$
$$\frac{\partial}{\partial z}[(\mu_m + \frac{\mu_t}{\sigma_\epsilon})\frac{\partial \epsilon}{\partial z}] + \frac{1}{r}\frac{\partial}{\partial r}[(\mu_m + \frac{\mu_t}{\sigma_\epsilon})\frac{\partial \epsilon}{\partial r}] \quad (7)$$

Current continuity equation

$$\frac{\partial}{\partial z}(\sigma\frac{\partial\phi}{\partial z}) + \frac{1}{r}\frac{\partial}{\partial r}(\sigma r\frac{\partial\phi}{\partial r}) = 0 \quad (8)$$

where ρ denotes the fluid density, u the velocity component in the axial direction (z), v the velocity component in the radial direction (r), w the velocity component in the azimuthal direction (θ), p the pressure, μ the apparent viscosity ($= \mu_m + \mu_t$), μ_m the fluid viscosity, j_z the axial component of current density, j_r the radial component of current density, B_θ the self-induced magnetic field in the radial direction, h the enthalphy, S_R the radiation loss, k the thermal conductivity, T the temperature, k_B the Boltzmann constant, e the electric charge, K the turbulent kinetic energy, ϵ the dissipation rate of K, G the energy production due to turbulence [3], μ_t the turbulent viscosity ($= c_\mu\rho K^2/\epsilon$), ϕ the electric potential, σ the electric conductivity, (c_μ, σ_K, σ_ϵ, $c_{\epsilon 1}$, $c_{\epsilon 2}$) the constants of turbulence model [4] and $|\dot\gamma|$ the magnitude of shear rate. The current density j_z and j_r are determined by the Ohm's law:

$$j_z = -\sigma\frac{\partial\phi}{\partial z}, \qquad j_r = -\sigma\frac{\partial\phi}{\partial r} \quad (9)$$

The self-induced magnetic field B_θ is calculated according to the Biot-Savart law:

$$B_\theta = \frac{\mu_0}{r}\int_0^r j_z\,\xi\,\mathrm{d}\xi \quad (10)$$

3. Kinetic model

The transport equation to describe the neutral species arising in the destruction process is given as follows:

$$\nabla\cdot(n_i\mathbf{U}) + \nabla\cdot\mathbf{\Gamma}_i = R_{i,p} + R_{i,d} \quad (11)$$

where n_i denotes the density of the ith species, $\mathbf{U}$ the flow velocity, $\mathbf{\Gamma}_i$ the flux of the ith species, $R_{i,p}$ the production of the ith species, $R_{i,d}$ the destruction of the ith species. The decomposition mechanism of fluorinated compounds disclosed in [1] together with the kinetic model for water plasma suggested in [5] is adopted in this paper to describe the perfluorocarbons decomposition in nitrogen thermal plasma. The following table summarizes the decomposition mechanisms for CF_4 considered in this study.

No.	Reactions
1	$CH_2F_2 + H \rightarrow CH_2F + HF$
2	$CF_4 + H \rightarrow CF_3 + HF$
3	$CF_4 \rightarrow CF_3 + F$
4	$CH_2F + F \rightarrow CHF + HF$
5	$CF_3 + O \rightarrow COF_2 + F$
6	$CF + O \rightarrow CO + F$
7	$CF_2 + O \rightarrow CO + 2F$
8	$CF_3 + H \rightarrow CF_2 + HF$
9	$CF_2 + H \rightarrow CF + HF$
10	$CF + H \rightarrow CH + F$
11	$CF_2 + F \rightarrow CF_3 + M$
12	$CF_3 + F \rightarrow CF_4 + M$
13	$CF_2 + H_2 \rightarrow CH_2F_2$
14	$CF_3 + H_2 \rightarrow CHF_3 + H$
15	$CF_2 + O_2 \rightarrow COF_2 + O$
16	$COF_2 + H \rightarrow COF + HF$
17	$COF_2 + O \rightarrow CO_2 + F_2$
18	$COF + O \rightarrow CO_2 + F$
19	$COF + H \rightarrow CO + HF$
20	$COF + F \rightarrow CO + F_2$

Table 1. Decomposition mechanisms for CF_4.

4. Numerical method

A finite volume method [6] is employed to discretize the governing differential equations on a Cartesian grid and then a integral form of governing equation over an arbitrary control volume V is obtained:

$$\int_S \rho\varphi(\mathbf{U}\cdot\mathbf{n})\,\mathrm{d}S = \int_S (\mathbf{T}_\varphi\cdot\mathbf{n})\,\mathrm{d}S + \int_V \rho f_\varphi\,\mathrm{d}V \quad (12)$$

where the control volume V is defined by the control surface S with an outer normal vector $\mathbf{n}$, φ the generalized variable, $\mathbf{U}$ the velocity vector, $\mathbf{T}_\varphi$ the generalized surface force, f_φ the generalized source term. Using the value of neighboring nodes to approximate each term appearing in the governing equations, a linearized equation is obtained for every governing equation. A SIMPLE-like algorithm is employed to solve the coupling of dependent variables iteratively. For the current density distribution at cathode, an exponential profile is assumed as follows [7]:

$$j_c(\xi) = J_{\max}\,\mathrm{e}^{-b\xi} \quad (13)$$

where $J_{\max}$ denotes the maximum current density, ξ the decreasing direction of current density and the constant b is determined by the system current I and the area of hot spot A:

$$I = 2\pi\int_A j_c(\xi)\,\mathrm{d}A \quad (14)$$

5. Boundary conditions

In the numerical modeling, the DC torch is simplified as a hollow cylinder with length of 89 mm and radius of 12 mm, Fig. 1. One end of the hollow cylinder
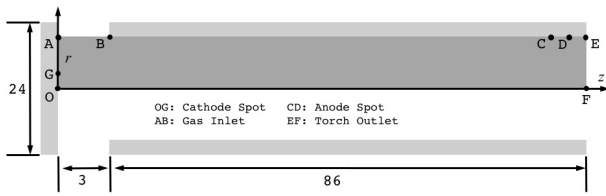
Figure 1. Computational domain and the location of electrodes.

is closed, while the other end is open for outgoing plasma. The inlet boundary conditions are specified at the annular gas inlet adjacent to the torch bottom. The flow rate of nitrogen is 180 slpm and a swirler design additionally yields a tangential velocity of 20 m/s at the gas inlet. CF_4 and H_2O are supplied together with the working gas (nitrogen) in a concentration of 10^4 ppm and $2 \cdot 10^4$ ppm, respectively. The working current of the simulated case is 145 A, which results in a measured voltage drop of 194 V between two electrodes. The location of cathode is at the center of torch bottom due to the installment of a cylindrical cathode. Anode's position is then fixed by the measured voltage obtained in the experiment. The arc root sizes of both electrodes are assumed 3 mm. About fifty thousand cells are used to discretize the computational domain, where the grid points close to arc root and gas inlet, as well as the torch wall, are clustered to resolve the steep gradient of field variables, such as velocity, temperature and current density.

6. Numerical results

Figure 2 depicts the plasma temperature and velocity profile at the torch outlet, where the predicted voltage drop is 191 V. The exiting plasma flow is accelerated by the self-induced magnetic field to deliver a blunt axial velocity profile. Except in the region close to torch wall ($r > 10$ mm), the nitrogen plasma can reach the speed range above 45 m/s along with a maximum value of 72 m/s at the centerline. Due to the installation of swirler at the gas inlet, a strong rotational flow in introduced into the hollow torch. The peak of tangential velocity is predicted for about 39 m/s located at about one third of the torch radius (4 mm). The position of the maximum tangential speed clearly defines the size of plasma core, which owns a relatively high velocity as well as temperature when compared with its outer region. Inside the core region, the plasma jet can attain a flow velocity over 60 m/s, whereas the temperature profile is between 3300 K and 7200 K. Figure 3 shows the plasma characteristics along the centerline. Because cathode is installed at the torch bottom, high current density and temperature as well as significant axial velocity is expected in the vicinity of the torch bottom. The spike of current density is predicted to be 62 A/mm², which gives a maximum temperature of 26000 K along the centerline. The axial velocity along the torch axis strongly oscillates as

the plasma moves away from the torch bottom. The flow quickly soars from -50 m/s to 290 m/s near the torch end, and substantially loses its velocity magnitude at approximately one-third of the torch length. With the help of nontrivial current density existing in the middle part of plasma torch, the plasma jet obtains an obvious velocity increase and exits from the torch at 90 m/s. Figure 4 illustrates the plasma characteristics inside the plasma torch. The right part of the figure disclose the velocity distribution, where a nontrivial vortex motion with the center located about 25 mm in front of the cathode is observed in the neighborhood of cathode. The temperature field as well as the current density vector is given in the left part of the figure. Significant current density emerges in the high-temperature core along the centerline.

Figure 5 gives the radial density profile of various species stemming from the decomposition mechanism of CF_4, where low density products are neglected in the profile plot. Water is relatively abundant (between 200 mole/cm³ and 300 mole/cm³) and smoothly distributed in the outer region of torch outlet ($r > 5$ mm), whereas it rapidly decline with the decrease of radial distance. Similar behavior is observed for CF_4, and at the same radial position the density of CF_4 is about one tenth of the water density. CF_3 as well as CH_2F shows a very low concentration in the plasma core, whereas an exponential grow of density is expected outside the hot plasma core. In contrast, the predicted density of fluorine atom varies in the range between 7 mole/cm³ and 20 mole/cm³ in the plasma core but a strong fall of concentration is predicted outside the high-temperature zone. The product group, i.e., HF, CO, and CHF, also deliver a hill-shape profile along the radial direction, where the peak density approximately occurs near the radial boundary of the plasma core. CHF_3 is the only material given in the profile plot, which exhibits a consistent tendency of growing concentration with r. The efficiency of CF_4 decomposition η in the investigated torch arrangement is 97%, where η is defined as the ratio of the mass flux at the gas inlet to the mass flux at the torch outlet

$$\eta = \frac{\dot{m}_{CF_4}|_{inlet}}{\dot{m}_{CF_4}|_{outlet}} \tag{15}$$

7. Conclusions

This paper proposes a numerical model to simulate the perfluorocarbons decomposition within a well-type, non-transferred nitrogen torch. An operation condition of 180 slpm, 145 A and 193 V is predicted using nitrogen as background gas, where water vapor and Tetrafluoromethane are initially with a concentration of 10^4 ppm and $2 \cdot 10^4$ ppm, respectively, at the gas inlet. The numerical simulation predicts the major products stemming from the decomposition mechanism of CF_4 are H_2O, F, HF, CO, CHF , CH_2F, CF_3,

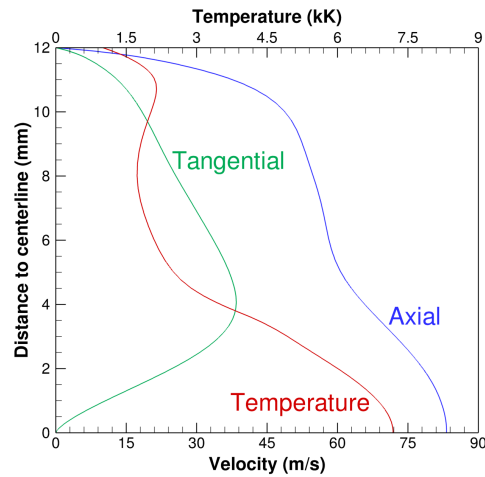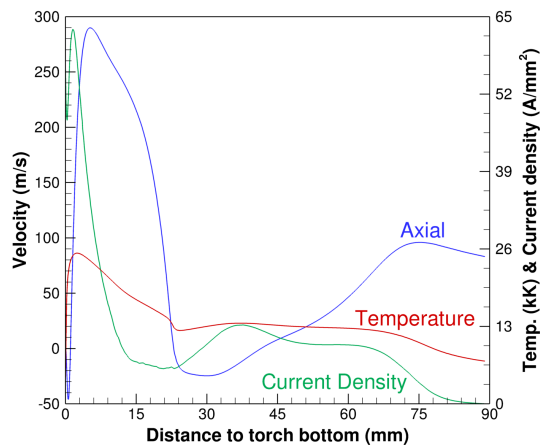*Figure 2. Plasma temperature and velocity profile at the torch outlet.*

Figure 3. Plasma characteristics along the centerline.

CF_4 and CHF_3. The efficiency of CF_4 decomposition via a nitrogen plasma torch under the studied operation condition is estimated about $97\,\%$.

Acknowledgements

References

[1] S.H. Narengerile and T. Watanabe. Decomposition mechanism of fluorinated compounds in water plasmas generated under atmospheric pressure. *Plasma Chem. Plasma Process*, 30(6):813–829, 2010. `doi:10.1007/s11090-010-9259-y`.

[2] M.S. Lim, S.C. Kim, and Y.N. Chun. Decomposition of PFC gas using a water jet plasma. *J. Mech. Sci. Tech.*, 25(7):1845–1852, 2011. `doi:10.1007/s12206-011-0422-z`.

[3] S.W. Chau, S.Y. Lu, and P.J. Wang. Modeling of axis-symmetric steam plasma flow in a non-transferred torch. *Comp. Phys. Comm.*, 182(1):152–154, 2011. `doi:10.1016/j.cpc.2010.08.011`.

[4] B.E. Launder and D.B. Spalding. The numerical computation of turbulent flows. *Comp. Methods in*
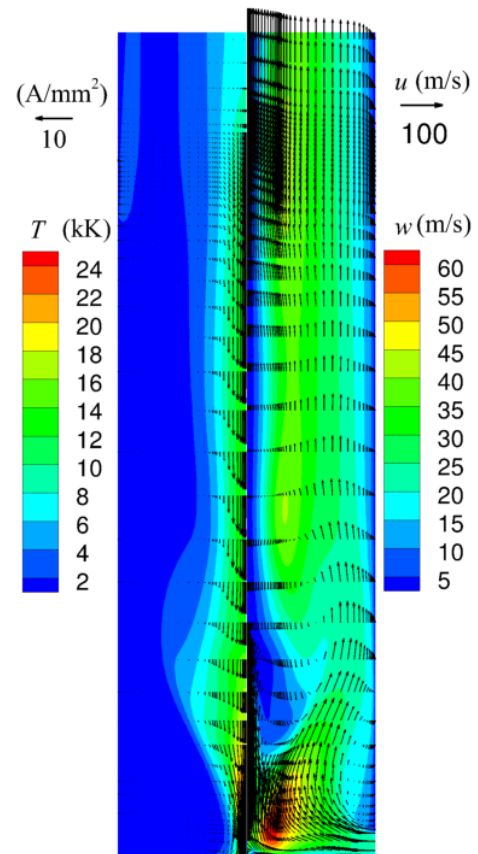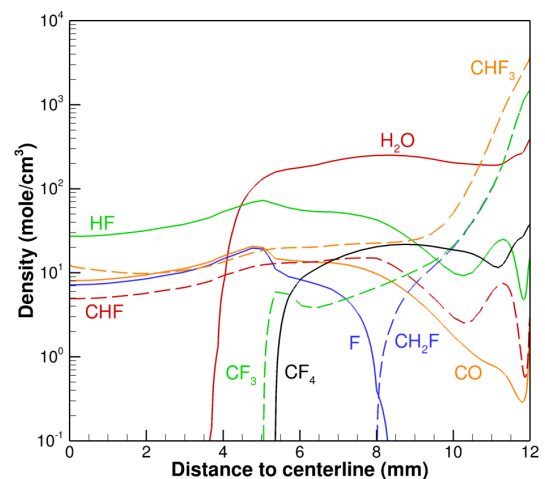

Figure 4. Plasma characteristics inside the torch.

Figure 5. Density profile at the torch outlet.

Appl. Mech. Eng., 3(2):269–289, 1974. `doi:0.1016/0045-7825(74)90029-2`.

[5] S.W. Chau, C.M. Tai, and S.H. Chen. Nonequilibrium modeling of steam plasma in a nontransferred direct-current torch. *IEEE Tran. Plasma Sci.*, 42(12):3797–3808, 2014. `doi:10.1109/TPS.2014.2365479`.

[6] S.W. Chau. *PhD Disseration*. Universität Hamburg, 1997.

[7] K.C. Hsu, K. Etemadi, and E. Pfender. Study of the free-burning high-intensity argon arc. *J. Appl. Phys.*, 54(3):1293–1301, 1983. `doi:10.1063/1.332195`.